

PHERMEX ELECTRON GUN DEVELOPMENT

L. A. Builta, J. C. Elliott, D. C. Moir,
T. P. Starke, and C. A. Vecere
Los Alamos National Laboratory
Los Alamos, NM 87545

Introduction

The PHERMEX facility is a 50-MHz standing wave linear accelerator. Electrons are injected, accelerated, and transported to a tungsten target where Bremsstrahlung x rays are generated for flash radiography of hydrodynamic systems. The machine is described in Ref. 1 and more recently Ref. 2.

The purpose of this article is to describe the progress of PHERMEX electron gun development. The goal of this program is to generate and transport a 200-ns, 1-MV, 1-kA electron beam into the first PHERMEX accelerating cavity. The standard gun is operated at a pulse voltage of 550 kV, which is the limit determined by internal breakdown of the vacuum insulator. This insulator has been redesigned, and the gun has been pulsed at 750 kV without internal breakdown. Characterization of the standard gun is described in Ref. 3.

At present, the current output is not limited by voltage but by a phenomenon called pulse shortening, which occurs at a pulse voltage of approximately 650 kV. The phenomenon has been investigated and the results are presented.

Experimental Arrangement

A schematic of the electron gun injector lens assembly is shown in Fig. 1. Electrons are generated on the 100-mm-diam hot cathode, made of a tungsten matrix impregnated with barium oxide. The electrons are extracted from the cathode and through the anode by a high-voltage pulse introduced in the back of the gun. The resulting beam is transported and focused by solenoidal magnets into the first accelerating cavity of PHERMEX. The emittance mask in the schematic is the location of the entrance to this cavity. The new convoluted vacuum insulator is shown in the schematic.

The solenoidal focusing elements contain copper coils with an Armco iron housing and field shaper. Each lens contains an aluminum gap 24 mm long. The upstream lens (L1) has the pole piece centered inside the magnet and is located 0.614 m from the surface of the cathode. The downstream lens (L2) has an offset pole piece and is located 1.151 m from the cathode surface. The solenoidal magnets were mapped prior to the experiments. Figure 2 is a graph of the peak magnetic field as a function of magnet current for both L1 and L2. Field shapes are shown in Ref. 1. The effective length of the lens, L, is given by (Ref. 4)

$$L = \frac{1}{B_m^2} \int_{-\infty}^{\infty} B(z)^2 dz$$

If B(z) is of the form

$$B(z) = \frac{B_m}{(1 + \frac{z^2}{a^2})} \text{ (Ref. 4) ,}$$

then the expression for L is

$$L = \frac{\pi a}{2} \approx 95 \text{ mm}$$

where $a \approx 60$ mm as determined from the field map of B(z) for currents between 1 and 7 amperes. For the experiments reported here, the lenses were operated at 5 A or less.

An electrical schematic of the gun-pulser is shown in Fig. 3. The Femcor is a coaxial cable Marx generator. It has a nominal pulse voltage duration of 200 ns; in practice the pulse length at full voltage is 150 ns because of rise- and fall-time considerations. For a matched load at 600 kV, the pulser is charged to 110 kV. In order to increase the gun voltage, the load resistance is increased; thus the pulser is mismatched to the gun/load resistor combination. The 110 kV charge voltage in these experiments gives 750 kV pulse voltage. The absolute voltage on the gun is monitored by the current viewing resistor (CVR) in series with the load resistor. All gun monitors are shown in Fig. 3 schematic. These include 1) capacitive voltage or V-dot probe located in a SF₆ bag on the back of the gun, 2) internal V-dot probe located inside the vacuum chamber at the A-K gap, 3) internal magnetic sense or B-dot loop located adjacent to the internal V-dot probe, 4) drift section B-dot loop located just downstream of the A-K gap, and 5) the emittance mask, which serves as a charge collector because it subtends 98% of the beam. All of the V-dot and B-dot signals are integrated at the input to the oscilloscopes using passive integrators. A camera was used to photograph the beam pattern transmitted through the emittance mask as in Ref. 3.

Measurement Results

The pulse voltage was varied between 440 kV and 750-kV. At each charge voltage the absolute pulse voltage was measured using the current viewing resistor (CVR). This monitor was cross calibrated with both of the integrated V-dot probes, which were used as relative monitors. These probes correlated linearly with each other and the CVR to within 4%. Table I, column 1 summarizes the pulse voltage data. All of the pulse amplitude measurements were made 150 ns from the start of the pulse.

The electron beam current both injected and transported through the solenoidal lenses is given in columns 3 and 4 of Table I. The emittance mask was used to monitor absolute beam current. Two integrated B-dot loops were relative monitors of the current and were cross correlated with the emittance mask/charge collector. The B-dot loops were only reliable at pulse voltages of less than 600 kV. Up to this voltage, the B-dot loop monitors correlated with the emittance mask measurement to within 5%. The measured current is corrected for backscatter from the aluminum emittance mask (~10% at all voltages and transmission through the slots and holes (~2%). Columns 4 and 5 are the pulse width of the current pulse at 80% of the current measured at the 150-ns point. Data are shown for both injected and transported current. The calculated perveance is given at the bottom of Table I. Figure 4 is a photograph of oscilloscope measurements of the different current and voltage monitors at 650-kV. All of the measurements were made simultaneously on a single pulse.

The emittance was measured at two locations, upstream and downstream of the solenoidal magnets. The upstream measurement was made with both lenses removed. A separate emittance mask drift section was attached to the short drift tube section between the gun and the lenses. The measurement was made 364 mm from the surface of the cathode. This location is shown on Fig. 1. The downstream measurement was made 1.54 m from the cathode surface and at the location of the PHERMEX accelerator cavity entrance. The results at 650-kV for injected beam are given in Fig. 5. The lenses were tuned so that L1 peak field was 0.034 T and L2 was 0.030 T for the transmitted beam measurements.

The results in columns 4 and 5 indicate that at voltages greater than 650 kV without the lenses and 685 kV with the lenses, we observe something we call pulse shortening. Figure 6 (b) and 6 (d) are two beam current pulses measured by the emittance mask at 650 kV and 685 kV, respectively. Clearly the pulse is shortened in length. This phenomena was observed in experiments where the anode aperture was 50.8 mm in diameter. By varying both the pulse voltage (charge pulse voltage and current (cathode temperature), we found that the threshold for pulse shortening occurred at constant power. This threshold was found to be 600 kV at full current. We installed a 63.5-mm-diam anode and two monitors, voltage and current on the A-K gap (Ref. 5). The threshold for pulse shortening increased to 650 kV. The signal on the integrated internal B-dot increased or continued at the time that the pulse shortened. Using the full bandwidth of our Tektronix 7834 oscilloscopes, we were unable to observe a substantial rf signal on either the B-dot loop or the V-dot probe. The result of the B-dot measurement at 650 kV and 685 kV is given in Fig. 6 (a) and (c). It should also be noted that the threshold increased from 650 kV to 685 kV by the addition of the solenoidal focusing lenses. There is no evidence of insulator breakdown associated with the pulse shortening.

Discussion and Conclusions

The PHERMEX standard electron gun has successfully been operated at pulse voltages of 685 kV with a full width current pulse. It has been pulsed as high as 750 kV without observable insulator breakdown. The higher current and voltage beams have been transported through the solenoidal focusing elements used to inject into the first PHERMEX accelerating cavity. The beam loss in transport is relatively small (3-5%). The beam

current and emittance have been characterized at both the entrance and exit of the lenses package.

Two possible causes of pulse shortening are microwave instabilities and ion/plasma defocusing. Electron beam/cavity microwave instabilities could generate sufficiently intense microwave fields to disrupt the electron beam. Formation of a plasma at the emittance mask or the anode aperture could perturb the beam by emitting ions into the beam so as to over-focus the beam, or could disrupt the beam if the plasma expansion radically changes the A-K geometry. The most probable microwave frequencies were estimated to be approximately 10 GHz. The magnetic and electric field probes did not detect any microwave signals coincident with pulse shortening. To test the plasma formation hypothesis, gun voltage and current probes were examined. The gun voltage probe detected a small decrease in the gun voltage when pulse shortening occurred (10-15%). The gun current probe detected no pulse shortening. The gun current was enhanced when pulse shortening of the beam current at the emittance mask occurred. For higher gun voltages at which pulse shortening was more dramatic, the gun current probe indicated gun current continued hundreds of nanoseconds beyond the gun voltage pulse. This signal characteristic implies that a late time anode-cathode gap plasma short has occurred. From this, we conclude that the pulse shortening is a result of anode plasma formation. We are constructing a cathode field-forming electrode so that there is no current intercepted at the anode. This involves the design of a new field forming electrode.

References

1. Venable, D., "PHERMEX: A Pulsed High Energy Radiographic Machine Emitting X-Rays," Los Alamos Report LA 3241 (1967).
2. Starke, T. P., "PHERMEX Standing Wave Linear Accelerator," IEEE Trans. Nuc. Sci., Vol. NS-30 (1983).
3. Elliott, J. C., Faehl, R. J., Fullbright, H. J., Moir, D. C., and Swannack, C. E., IEEE Trans. Nuc. Sci., NS-28 (1981) p. 2699.
4. Fert, C. and Durandau, P., "Magnetic Electron Lenses," *The Focusing of Charged Particle Beam*, A. Septier, Ed., (Academic Press, New York, 1967), Vol. I, p. 309.
5. Reid, D. and Tallerico, P., private communication.

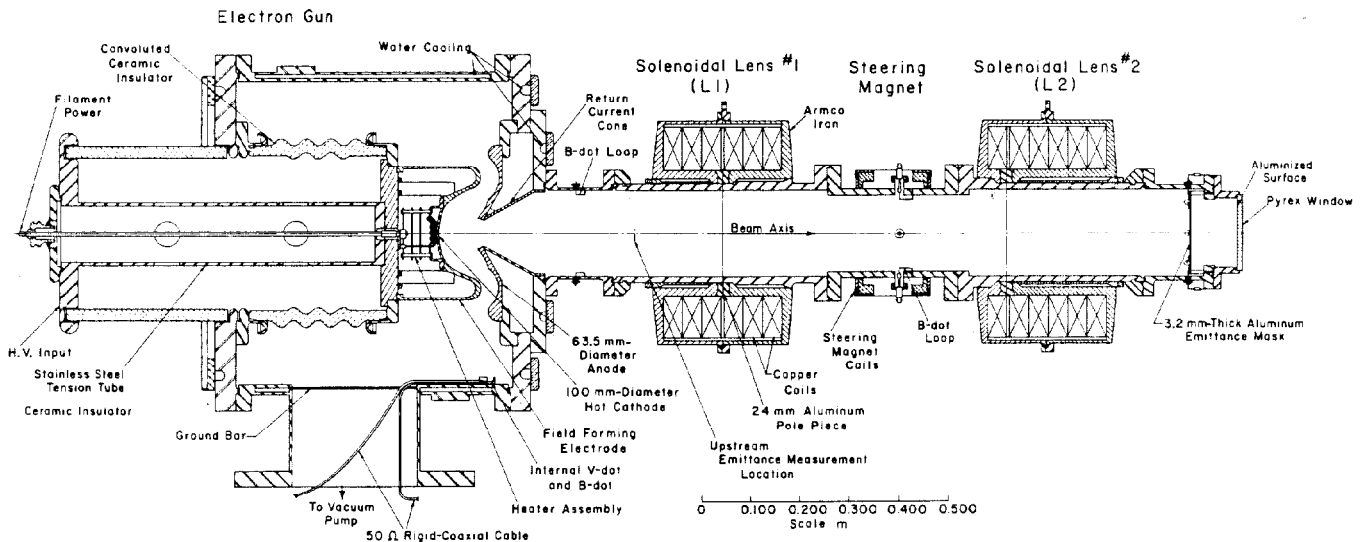


Fig. 1. Schematic of the electron-gun lens assembly with emittance mask.

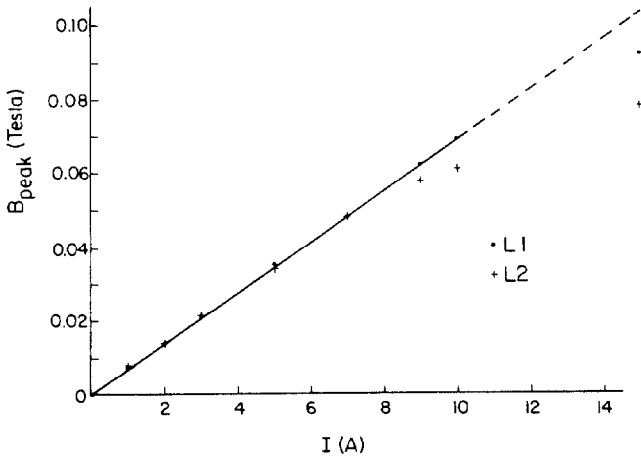


Fig. 2. Peak axial magnetic field in lenses L1 and L2 as a function of current.

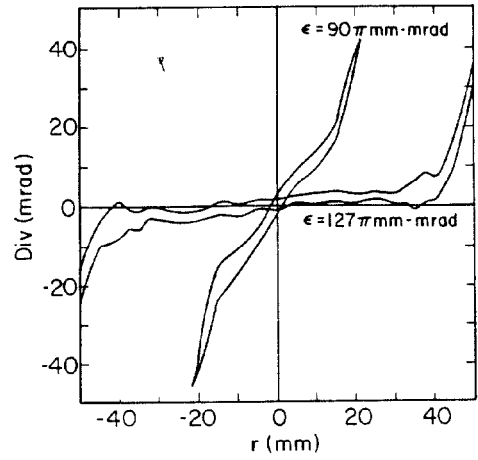


Fig. 5. Electron beam emittance at the entrance and exit of the solenoidal lenses.

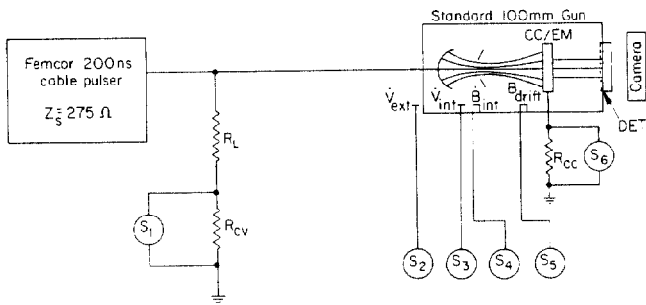


Fig. 3. Schematic of electron-gun pulser circuit with monitors.

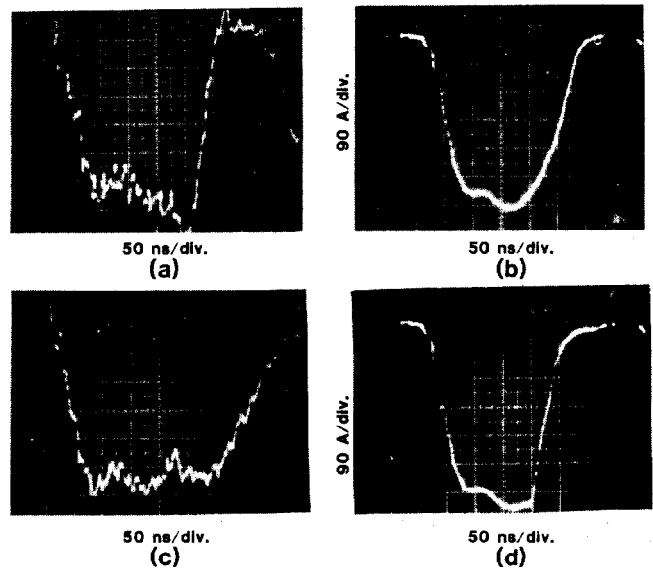


Fig. 6. Oscilloscope traces of the integrated internal B-dot loop and the emittance mask/charge collector.

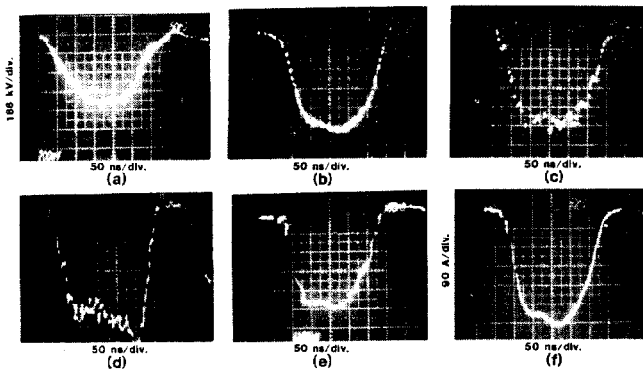


Fig. 4. Sample oscilloscope traces of a) CVR, b) integrated V-dot, c) integrated internal V-dot, d) integrated internal B-dot, e) integrated drift tube B-dot, f) emittance mask/charge collector at 650-kV pulse voltage.

TABLE I

Gun/Pulse (kV) ±15*	Injected Current (A) ±15*	Transported Current (A) ±15*	Injected Current Pulse Width @ 80% (ns) ±5*	Transported Current Pulse Width @ 80% (ns) ±5*
440	320	320	165	165
510	390	375	165	165
580	470	455	165	165
615	515	500	165	165
650	550	525	165	165
685	590	570	135	165
720	620	595	135	145
750	---	625	---	135

*Estimate of systematic error in acquiring and reading scope traces. $g_{ave} = 1.06 \pm 0.02 \mu P$ for all data at 150 μs .